

Coupling of Rotational Motion with Shape Fluctuations of Core-shell Microgels Having Tunable Softness

S. Bolisetty^a, M. Hoffmann^a, S. Lekkala^a, Th. Hellweg^a, M. Ballauff^a, and L. Harnau^b

^a*Physikalische Chemie I, University of Bayreuth, D-95440 Bayreuth, Germany*

^b*Max-Planck-Institut für Metallforschung, Heisenbergstr. 3, D-70569 Stuttgart, Germany,*

and Institut für Theoretische und Angewandte Physik,

Universität Stuttgart, Pfaffenwaldring 57, D-70569 Stuttgart, Germany

(Dated: November 18, 2018)

The influence of shape fluctuations on deformable thermosensitive microgels in aqueous solution is investigated by dynamic light scattering (DLS) and depolarized dynamic light scattering (DDLS). The systems under study consist of a solid core of polystyrene and a thermosensitive shell of cross-linked poly(N-isopropylacrylamide) (PNIPA) without and with embedded palladium nanoparticles. PNIPA is soluble in water, but has a lower critical solution temperature at 32 °C (LCST). Below the LCST the PNIPA shell is swollen. Here we find that besides translational and rotational diffusion, the particles exhibit additional dynamics resulting from shape fluctuations. This leads to a pronounced apparent increase of the rotational diffusion coefficient. Above the transition temperature the shell collapses and provides a rather tight envelope of the core. In this state the dynamics of the shell is frozen and the core-shell particles behave like hard spheres. A simple physical model is presented to capture and explain the essentials of the coupling of rotational motion and shape fluctuations.

I. INTRODUCTION

In recent years, a lot of research has been focused on the preparation and investigation of “smart” microgels consisting of a thermosensitive network of poly(N-isopropylacrylamide) (PNIPA).^{1,2,3,4,5,6,7} Major incentives for this research were possible applications in catalysis,⁶ photonics⁸ or for the fabrication of responsive surface coatings.⁹ In particular, core-shell particles consisting of a polystyrene core onto which a thermosensitive network is affixed present well-defined model colloids and exhibit polydispersities below $\pm 6\%$.^{10,11,12,13,14} Hence, besides their potential for applications these core-shell microgels are interesting model systems for studies of the flow behavior of concentrated colloidal suspensions.^{15,16} In this way core-shell microgels have become one of the best-studied class of polymer colloids.

In aqueous media, PNIPA exhibits a lower critical solution temperature (LCST) of about 32 °C.^{17,18,19,20,21} Below this temperature the network is swollen by the solvent water whereas water is expelled from the microgel above the lower critical solution temperature. Hence, in the swollen state the PNIPA shell of the core-shell microgels is expected to have a rather soft character. This implies the presence of network breathing modes in this state. Up to now, there is evidence that the rheology of colloidal suspensions is strongly related to the dynamic properties of these often deformable objects. An important example in this context represents the flow of blood, containing deformable erythrocytes. Other important examples are liquid droplets, emulsions, and vesicles. While experimental and theoretical studies have been devoted to the understanding of the dynamics of bending modes,^{22,23,24,25,26,27} the effect of shape fluctuations on the rotational diffusion coefficient of deformable objects has not been investigated yet despite

the importance of the rotational degree of freedom for soft materials.^{28,29,30,31} Possible reasons may be sought in the lack of well-defined monodisperse model systems that can be studied by suitable experimental techniques.

Here we study the translational and rotational motion of thermosensitive core-shell microgel particles by depolarized dynamic light scattering (DDLS).^{32,33} The aim of the present work is a better understanding of the coupling of rotational motion and shape fluctuations. Such microgels are highly suitable for the present study because these particles have been extensively studied by scattering methods such as small-angle neutron scattering, small-angle X-ray scattering, and light scattering.^{6,34,35,36,37,38,39,40,41} It has been demonstrated that metal nanoparticles can be embedded in the network of the shell.^{6,42,43} Moreover, recent work has shown that cryogenic transmission electron microscopy (Cryo-TEM) is well suited to study the structure and the shape of these particles in-situ.^{44,45} A thin film of the fluid dispersion containing the particles is shock-frozen and subsequently analyzed by transmission electron microscopy (TEM), no staining or any other preparatory step is necessary. Figure 1 shows typical cryo-TEM micrographs of dilute suspensions of such core-shell particles. The core consisting of polystyrene and the shell of cross-linked PNIPA is clearly visible. Figures 1 (a) and (c) display the bare particles at different temperatures while Figure 1 (b) shows a core-shell system where palladium nanoparticles are embedded in the shell.^{42,43} The shape of the core-shell microgels shown in Figures 1 (a) and (b) is slightly asymmetric. This asymmetry must be traced back to thermal fluctuations. Therefore, we expect the dynamic properties of the core-shell system to be influenced by the shape fluctuations of the shell. Depolarized dynamic light scattering (DDLS) is the method of choice for studying the problem at

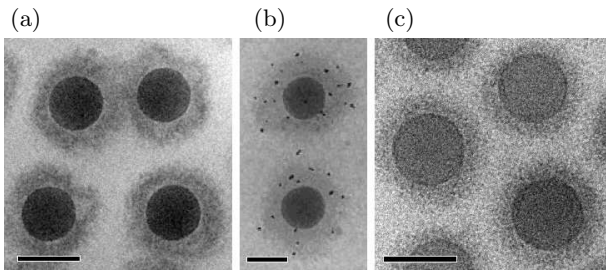


FIG. 1: CryoTEM micrographs of thermosensitive core-shell particles in aqueous solution. The samples were maintained at 25 °C in (a), (b) and at 45 °C in (c) before vitrification. The dark core consists of polystyrene and the corona of PNIPA cross-linked with N, N' -methylenebisacrylamide. In (b) palladium nanoparticles (black dots) are embedded in the PNIPA-shell.^{42,43} The scale bars are 100 nm.

hand since this technique simultaneously probes the translational and rotational diffusion coefficient of optically anisotropic particles.^{32,33} DDLS has been applied to a number of anisometric particles in dilute solution.^{46,47,48,49} In general, spherical particles should not exhibit a signal in DDLS. However, the shape fluctuations of the core-shell microgels that are visible as frozen anisometry in the Cryo-TEM micrographs (see Fig. 1) should lead to an optical anisotropy of sufficient magnitude to give a finite depolarized signal in solution. In addition, even in the absence of these shape fluctuations network inhomogeneities due to an anisotropic distribution of crosslinking points will give rise to an additional contribution in the DDLS intensity autocorrelation function. This is observed indeed. On the other hand, the average shape of the particles is still spherical and rather simple models can still be applied. This conclusion can be derived from the fact that these particles have the phase diagram of hard spheres.^{15,16}

The paper is organized as follows: After the section Experimental we first give a brief survey on the theory of DDLS and develop a general scheme for the evaluation of data. In a second step we discuss the intensity autocorrelation functions for the microgels above and below their transition temperature in terms of a slow and a fast relaxation rate, the latter being related to the coupling of shape fluctuations and rotational motion. In the last section a simple statistical-mechanical model is presented that provides a qualitative explanation of the experimental data.

II. EXPERIMENTAL

The synthesis and the characterization of the particles has been described previously.^{6,15,44} All solutions (0.05 wt %) were prepared in 0.05 M KCl to reduce electrostatic particle interactions^{15,16} and filtered into dust free

sample holders using 0.45 μm nylon filters.

All experiments were carried out using the ALV/DLS/SLS-5000 compact goniometer system equipped with a He-Ne laser ($\lambda = 632.8$ nm). The scattering cells (10 mm cylindrical cuvettes, Hellma) were immersed in an index matching bath of cis-decaline which does not change the polarization plane of the laser light as e.g. toluene. For the DDLS experiment, the primary beam and the scattered light passed through a Glan-Thomson polarizer with an extinction coefficient better than 10^{-5} . The first polarizer guaranteed that mainly vertically polarized light impinges on the sample and the orientation of a second polarizer (analyzer) was carefully adjusted to a crossed position with the minimum scattered intensity. All radii of the particles a given in the text were obtained by DLS.

III. INTENSITY AUTOCORRELATION FUNCTION

The theory of dynamic light scattering has been presented in various treatises.^{32,33} Hence, we only review the equations necessary for this study. For an incident light wave traveling in the x direction with a polarization vector in the z direction the intensity of the scattered electric field can be written as

$$I_s(\mathbf{q}, t) = I_{VV}(\mathbf{q}, t) + I_{VH}(\mathbf{q}, t), \quad (1)$$

where the absolute value of the scattering vector \mathbf{q} is given by $q = |\mathbf{q}| = (4\pi n/\lambda) \sin(\theta/2)$ in which n is the refractive index of the medium. λ is the incident wavelength and θ is the scattering angle. Pecora^{46,50} has given general expressions for $I_{VV}(\mathbf{q}, t)$ and $I_{VH}(\mathbf{q}, t)$ as

$$I_{VV}(\mathbf{q}, t) \sim \int d\mathbf{r} d\mathbf{r}' \langle \alpha_{zz}(\mathbf{r} + \mathbf{r}', t) \alpha_{zz}(\mathbf{r}', 0) \rangle e^{i\mathbf{q}\cdot\mathbf{r}}, \quad (2)$$

$$I_{VH}(\mathbf{q}, t) \sim \int d\mathbf{r} d\mathbf{r}' \langle \alpha_{zy}(\mathbf{r} + \mathbf{r}', t) \alpha_{zy}(\mathbf{r}', 0) \rangle e^{i\mathbf{q}\cdot\mathbf{r}}, \quad (3)$$

where $\alpha_{zz}(\mathbf{r}, t)$ and $\alpha_{zy}(\mathbf{r}, t)$ are the zz and zy elements of the fluid polarizability tensor. Experimentally accessible quantities are the intensity autocorrelation functions $g_{VV}^{(2)}(\mathbf{q}, t)$ using dynamic light scattering (DLS) and $g_{VH}^{(2)}(\mathbf{q}, t)$ using DDLS. For photon counts obeying Gaussian statistics, the intensity autocorrelation functions are related to the electric field autocorrelation functions $g_{VV}^{(1)}(\mathbf{q}, t)$ and $g_{VH}^{(1)}(\mathbf{q}, t)$ according to

$$g_{VV}^{(2)}(\mathbf{q}, t) = 1 + f_{VV} \left(g_{VV}^{(1)}(\mathbf{q}, t) \right)^2, \quad (4)$$

$$g_{VH}^{(2)}(\mathbf{q}, t) = 1 + f_{VH} \left(g_{VH}^{(1)}(\mathbf{q}, t) \right)^2, \quad (5)$$

where f_{VV} and f_{VH} are dependent on the scattering geometry and are usually treated as adjustable parameters. The electric field correlation functions can be calculated for various systems.

The core-shell particles in solution can change their position, orientation, and shape randomly by thermal agitation. For a dilute solution containing noninteracting monodisperse spherical particles of radius a the intensity autocorrelation functions are given by:

$$\sqrt{g_{VV}^{(2)}(q, t) - 1} = e^{-q^2 D_T(a)t}, \quad (6)$$

$$\sqrt{g_{VH}^{(2)}(q, t) - 1} = \frac{e^{-q^2 D_T(a)t} (B(q, a) + e^{-6D_R(a, \alpha)t})}{B(q, a) + 1}. \quad (7)$$

The translational and rotational diffusion coefficients read

$$D_T(a) = \frac{k_B T}{\eta} \frac{1}{6\pi a}, \quad (8)$$

$$D_R(a, \alpha) = \frac{k_B T}{\eta} \frac{1}{8\pi a^3} \alpha, \quad (9)$$

where the temperature T and viscosity η characterize the solvent and $\alpha = 1$ for hard spheres. The parameter $B(q, a)$ in eq 7 takes into account possible contributions of polarized components to the intensity of the scattered light in the DDLS experiment due to a limited extinction ratio of the polarizer as discussed below.

As a new feature of the present evaluation, we have introduced the parameter α in eq 9. This parameter describes the difference of the real system from the hard sphere model, that is, $\alpha = 1$: If $\alpha = 1$, the rotational diffusion as well as the translational diffusion is fully described by a single parameter, namely the hydrodynamic radius a . If $\alpha \neq 1$, the rotational diffusion is coupled to an additional degree of freedom of the particle. Since $D_R(a, \alpha)$ scales with a^{-3} , possible deviations may hence be determined by precise DDLS-measurements.

IV. RESULTS AND DISCUSSION

A. Microgels above the LCST

We first discuss the microgel particles at temperatures above the volume transition. Here we expect the dynamics of the core-shell particles at $T = 45^\circ\text{C}$ to be the same as those of hard spheres because the shell is fully collapsed under these conditions and provides a rather tight envelope of the core as is apparent from Figure 1 (c).⁴⁴ The tight and nearly homogeneous shell visible above the transition temperature can be traced back to the fact that the particles are synthesized at high temperatures (80°C).¹⁰ It must be kept in mind that the interaction between the particles becomes attractive above the transition temperature and the particles may coagulate slowly.¹⁵ However, the small concentrations used in the present DDLS experiments prevent this coagulation.

Figure 2 displays examples of measured and calculated intensity autocorrelation functions of the core-shell particles containing palladium nanoparticles at

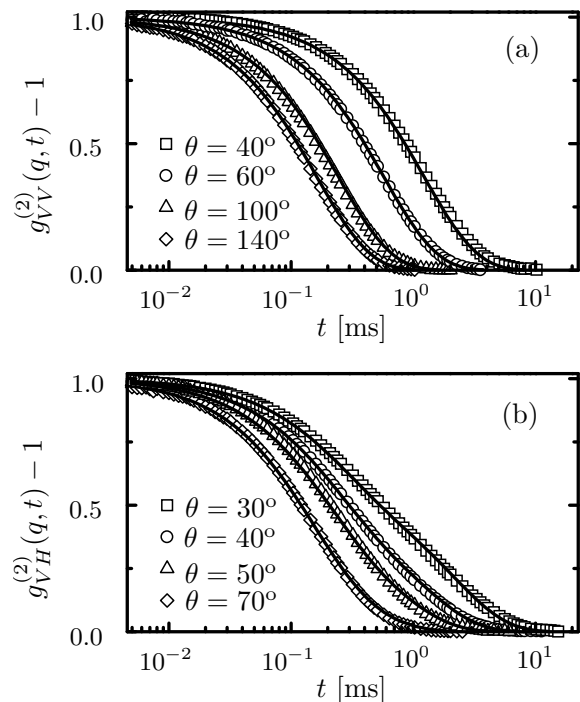


FIG. 2: (a) [(b)] DLS [DDLS] intensity autocorrelation functions $g_{VV}^{(2)}(q, t)$ [$g_{VH}^{(2)}(q, t)$] (symbols) of the core-shell particles containing palladium nanoparticles at $T = 45^\circ\text{C}$ (see Figure 1 (c)) together with the calculated results for monodisperse hard spheres (lines) according to eqs 6 - 9 with $a = 78$ nm and $\alpha = 1$. In (a) and (b) the scattering angle θ increases from right to left.

$T = 45^\circ\text{C}$. In the calculations the model parameters $\eta = 0.601 \times 10^{-3}$ Ns/m², $a = 78$ nm, and $\alpha = 1$ have been used. From both the translational and the rotational diffusion coefficient the same hydrodynamic radius of the microgel particles can be calculated (78 nm). The full agreement between the experimental data and the calculated results demonstrates that the theoretical approach according to eqs 6 - 9 for hard spheres is indeed appropriate for the microgel particles at high temperature. Moreover, it indicates that the residual polydispersity does not disturb the measurements.

B. Microgels below the transition

Figure 3 displays examples of measured and calculated intensity autocorrelation functions of the core-shell particles containing palladium nanoparticles at $T = 25^\circ\text{C}$. In the calculations the model parameters $\eta = 0.896 \times 10^{-3}$ Ns/m², $a = 115$ nm, and $\alpha = 1.6$ have been used. The radius agrees with the radius of the particles as obtained from the CryoTEM micrographs shown in Figures 1 (a) and (b). However, it turned out that a value of $\alpha = 1.6$ above unity had to be chosen in order to describe the experimental data. The value $\alpha = 1.6$ found

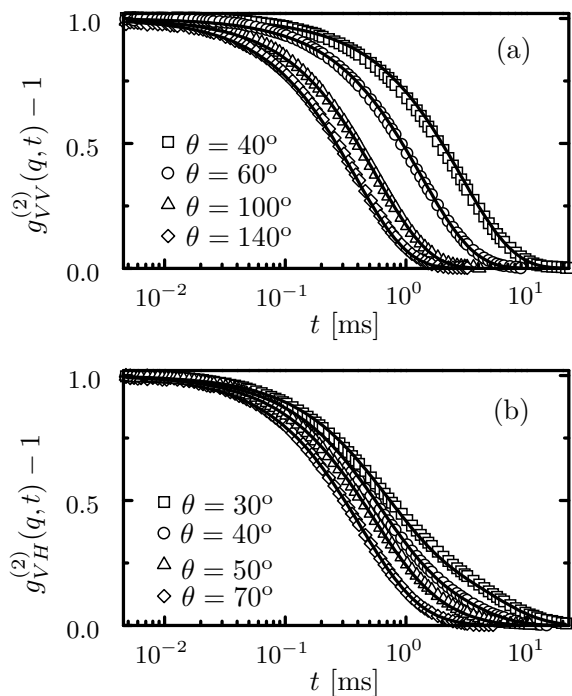


FIG. 3: (a) [(b)] DLS [DDLS] intensity autocorrelation functions $g_{VV}^{(2)}(q, t)$ [$g_{VH}^{(2)}(q, t)$] (symbols) of the core-shell particles containing palladium nanoparticles at $T = 25^\circ\text{C}$ (see Figure 1 (b)) together with the theoretical results (lines) as obtained from eqs 6 - 9 with $a = 115$ nm and $\alpha = 1.6$. In (a) and (b) the scattering angle θ increases from right to left.

temperature T	45°C	25°C	15°C
radius a [nm]	78	115	128
α	1	1.6	2.5
$D_R(a, \alpha)$ [s^{-1}]	611	192	168

TABLE I: The radius a of the core-shell particles containing palladium nanoparticles, the parameter α , and the diffusion coefficient $D_R(a, \alpha)$ as obtained from modelling experimental scattering data in terms of eqs 6 - 9. Above the transition temperature $T = 32^\circ\text{C}$ the dynamics of the core-shell particles is the same as those for hard spheres ($\alpha = 1$) because the shell provides a rather tight envelope of the core (see Figure 1 (c)). Below the transition temperature the particles exhibit additional dynamics resulting from shape fluctuations ($\alpha > 1$ and see Figures 1 (a) and (b)).

here indicates that the core-shell particles exhibit additional dynamics resulting from the shape fluctuations shown in Figures 1 (a) and (b). The difference between the measured DDLS data and the ones calculated from the hard sphere model increase upon decreasing the temperature. This is illustrated in Table I, where the parameter α is presented for three temperatures.

We have found that embedding nanoparticles in the network of the shell only weakly influences the dynamics of the core-shell particles as is apparent from Fig. 4. In

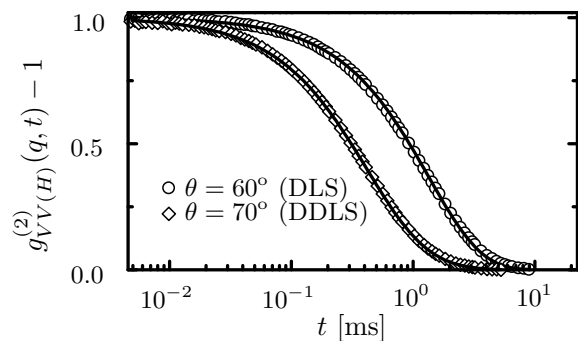


FIG. 4: Measured DLS (circles) and DDLS (diamonds) intensity autocorrelation functions $g_{VV}^{(2)}(q, t)$ and $g_{VH}^{(2)}(q, t)$ of the core-shell particles without embedded palladium nanoparticles at $T = 25^\circ\text{C}$ (see Figure 1 (a)) together with the same theoretical results (lines) used in Fig. 3 for the core-shell particles containing palladium nanoparticles at $T = 25^\circ\text{C}$.

this figure examples of measured DLS and DDLS intensity autocorrelation functions of the core-shell particles without embedded palladium nanoparticles at $T = 25^\circ\text{C}$ are shown together with the theoretical results (lines) already used in Fig. 3 that refer to core-shell particles containing palladium nanoparticles. Both measurements refer to the same temperature and the comparison demonstrates that the embedded nanoparticles do not disturb the volume transition of the thermosensitive network. No additional crosslinking or influence of the nanoparticles on the polymer chains in the network is seen in full accord with previous findings.^{42,43}

C. Slow and fast mode

The autocorrelation function $\sqrt{g_{VH}^{(2)}(q, t) - 1}$ in eq 7 is a sum of two discrete exponentially decaying functions, where the slow relaxation mode characterizes translational diffusion while the faster relaxation mode is related to rotational motion and shape fluctuations. Hence, one may describe the experimental data in terms of a slow (Γ_{slow}) and a fast relaxation rate (Γ_{fast}) according to

$$\Gamma_{slow}(q, a) = q^2 D_T(a), \quad (10)$$

$$\Gamma_{fast}(q, a, \alpha) = q^2 D_T(a) + 6D_R(a, \alpha). \quad (11)$$

The slow mode is also characteristic for the single exponential decay of the autocorrelation function $\sqrt{g_{VV}^{(2)}(q, t) - 1}$ in eq 6. Figure 5 shows the calculated relaxation rates as a function of q^2 . The solid and dotted lines denote $\Gamma_{slow}(q, a)$ and $\Gamma_{fast}(q, a, \alpha = 1)$, respectively, where $a = 78$ nm at $T = 45^\circ\text{C}$ in (a) and $a = 115$ nm at $T = 25^\circ\text{C}$ in (b). The hard sphere model, i.e., $\alpha = 1$, is indeed appropriate for the microgel particles at $T = 45^\circ\text{C}$ as discussed above and apparent from a comparison of the calculated results (solid and dotted

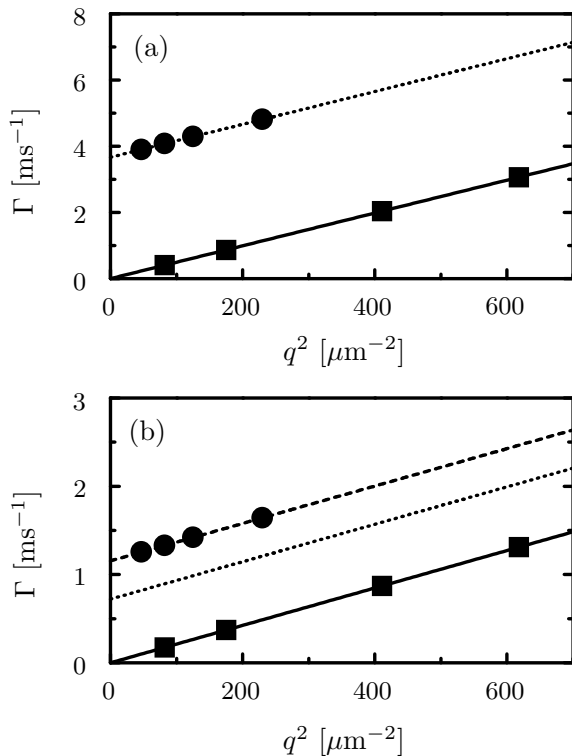


FIG. 5: Decay rates $\Gamma_{slow}(q, a)$ (solid lines), $\Gamma_{fast}(q, a, \alpha = 1)$ (dotted lines), and $\Gamma_{fast}(q, a, \alpha = 1.6)$ (dashed line) in (b) as calculated according to eqs 10 and 11. The squares and circles denote the slow and fast relaxation rate, respectively, used to describe the intensity autocorrelation functions of the core-shell particles containing palladium nanoparticles (see Figures 2 and 3) at $T = 45^\circ\text{C}$ in (a) and $T = 25^\circ\text{C}$ in (b). The absolute value of the scattering vector is given by $q = 26.45 \sin(\theta/2) \mu\text{m}^{-1}$ where θ is the scattering angle. Hence $q^2 = 618 \mu\text{m}^{-2}$ corresponds to $\theta = 140^\circ$.

lines) with the experimental data (symbols) in Figure 5 (a). The pronounced differences between the calculated decay rates $\Gamma_{fast}(q, a, \alpha = 1)$ (dotted line) and the experimental data (circles) in Figure 5 (b) are due to the shape fluctuations at $T = 25^\circ\text{C}$. Therefore, the value $\alpha = 1.6$ (see Table I) has been used in computing the dashed line displaying $\Gamma_{fast}(q, a, \alpha = 1.6)$.

We emphasize that neither modeling the core-shell particles as hard nonspherical particles such as ellipsoids or dimers nor taking into account the small size polydispersity of the particles or intermolecular interactions lead to an agreement with the experimental data. For example, the corresponding diffusion coefficients of a hard dimer consisting of two identical hard spheres of radius a are given by $D_T^{(dim)}(a) = 0.718 D_T(a)$ and $D_R^{(dim)}(a) = 0.265 D_R(a)$, respectively.⁵¹ Hence the ratio of the rotational diffusion coefficient to the translational diffusion coefficient D_R/D_T is smaller for hard dimers than for hard spheres, while the opposite behavior has been found for the core-shell particles below the transition temperature.

Size polydispersity of the particles leads to a considerably slower decay of the intensity autocorrelation functions⁵² in comparison with both the corresponding autocorrelation functions of a monodisperse system and the experimental data. Moreover, D_T and D_R decrease with increasing volume fraction of hard spheres.⁴⁹ Hence, this comparison demonstrates clearly that the dynamics of the core-shell particles below the transition temperature cannot be explained in terms of a hard particle model.

Furthermore, the experimental results cannot be explained by using slipping boundary conditions (see, e.g., ref⁵³) instead of the conventional sticking boundary conditions which lead to eqs 8 and 9. The translational diffusion coefficient of a sphere with slipping boundary conditions is increased by the factor $3/2$ as compared to $D_T(a)$ in eq 8, while the rotational motion of such a sphere does not displace any fluid, implying that $D_R(a) \rightarrow \infty$. Both results do not agree with the experimental data.

D. Coupling of the shape fluctuations with rotational motion

In the following we present a model that takes into account the influence of shape fluctuations on the rotational motion of the particles. As is illustrated in Figure 6, the motion of a scattering unit (solid circle) on a PNIPA chain within the shell of the particles can be decomposed into various types of modes. If the shell provides a rather tight envelop of the core, the scattering unit will exhibit translational motion and rotational motion around the center of mass of the particle (Figure 6 (a)), that is, the particles will behave as hard spheres without internal degrees of freedom. So above the LCST the DDLs signal will be due to the inhomogeneity of the frozen polymer network. However, there is an additional fluctuation dynamic (fluct; see Figure 6) due to internal degrees of freedom of the PNIPA chain if the shell is rather soft (Figure 6 (b)).

In the following we shall discuss the coupling between the rotational dynamics and the internal modes of the particles that come into play below the transition temperature. The PNIPA chains are linear chain molecules which are described by a chain model for macromolecules of variable stiffness^{54,55} that has been used earlier to discuss the dynamics of polymers under the influence of various forces (see, e.g., refs^{56,57,58,59} and references therein). It has been shown that the dynamics of individual PNIPA chains in dilute solution can be interpreted in terms of a chain model of this type.⁶⁰ We consider a continuous, differentiable space curve $\mathbf{r}(s, t)$ inscribed into a sphere of radius a , where $s \in [-a, a]$ is a coordinate along the macromolecule and $\mathbf{r}(0, t)$ is the position vector of the center of the sphere (see Figure 6). The potential energy

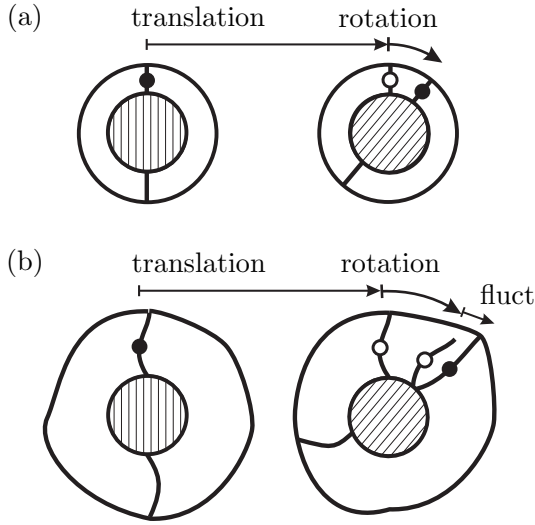


FIG. 6: Illustration of the motion of a scattering unit (solid circle) on a PNIPA chain within the shell of the core-shell particles, where the hatched region marks the core of the particles. The scattering unit exhibits translational motion and rotational motion around the center of mass of the particle in the case of a rather tight shell in (a), while there is an additional fluctuation dynamics (fluct) due to internal degrees of freedom of the PNIPA chain if the shell is rather soft in (b).

functional of the model reads^{54,55}

$$\begin{aligned}
 U_{pot}[\mathbf{r}(s, t)] = & \\
 & \int_{-a}^a ds \left[\nu p(s) \left(\frac{\partial \mathbf{r}(s, t)}{\partial s} \right)^2 + \frac{\epsilon}{p(s)} \left(\frac{\partial^2 \mathbf{r}(s, t)}{\partial s^2} \right)^2 \right] \\
 & + \nu_0 \left[\left(\frac{\partial \mathbf{r}(-a, t)}{\partial s} \right)^2 + \left(\frac{\partial \mathbf{r}(a, t)}{\partial s} \right)^2 \right], \quad (12)
 \end{aligned}$$

where $1/p(s)$ is a local correlation length characterizing the stiffness of the space curve and ν_0, ν, ϵ are Lagrange multipliers. In the limit $p(s) \rightarrow 0$, the space curve describes a rigid vector inscribed into a hard sphere which exhibits translational and pure rotational Brownian motion. Internal fluctuation of the PNIPA chains are taken into account in terms of $p(s) \neq 0$ for values of s inside the shell. The term with the first derivative in $\mathbf{r}(s, t)$ captures the chain flexibility, i.e., it takes chain entropy into account. The term with the second derivative accounts for bending stiffness and the last two terms are due to the broken symmetry at the chain ends⁵⁴. In order to gain analytical insight we consider the case that the flexibility parameter $p(s)$ does not depend on s , that is, $p(s) = p$. Applying Hamilton's principle we find the Langevin equation of motion along with the boundary

conditions for free ends,

$$3\pi\eta \frac{\partial}{\partial t} \mathbf{r}(s, t) - 2\nu p \frac{\partial^2}{\partial s^2} \mathbf{r}(s, t) + \frac{\epsilon}{p} \frac{\partial^4}{\partial s^4} \mathbf{r}(s, t) = \mathbf{f}(s, t), \quad (13)$$

$$\left[2\nu p \frac{\partial}{\partial s} \mathbf{r}(s, t) - \frac{\epsilon}{p} \frac{\partial^3}{\partial s^3} \mathbf{r}(s, t) \right]_{\pm a} = 0, \quad (14)$$

$$\left[2\nu_0 \frac{\partial}{\partial s} \mathbf{r}(s, t) + \frac{\epsilon}{p} \frac{\partial^2}{\partial s^2} \mathbf{r}(s, t) \right]_a = 0, \quad (15)$$

$$\left[2\nu_0 \frac{\partial}{\partial s} \mathbf{r}(s, t) - \frac{\epsilon}{p} \frac{\partial^2}{\partial s^2} \mathbf{r}(s, t) \right]_{-a} = 0, \quad (16)$$

where $\mathbf{f}(s, t)$ is the stochastic force. The first term in eq 13 represents the frictional force. Equation 13 is a fourth-order, linear partial differential equation which can be solved by means of a normal mode analysis. The eigenvalue problem including the boundary conditions is hermitian. Therefore, the eigenfunctions $\psi_l(s)$ are orthogonal and form a complete set. An expansion of the position vector and of the stochastic force in terms of the eigenfunctions and the time-dependent amplitudes $\chi_l(t)$, $\mathbf{f}_l(t)$ according to $\mathbf{r}(s, t) = \sum_{l=0}^{\infty} \psi_l(s) \chi_l(t)$ and $\mathbf{f}(s, t) = \sum_{l=0}^{\infty} \psi_l(s) \mathbf{f}_l(t)$ yields

$$\begin{aligned}
 \mathbf{r}(s, t) = & \sum_{l=1}^{\infty} \frac{\psi_l(s)}{3\pi\eta} \int_{-\infty}^t dt' \mathbf{f}_l(t') e^{-(t-t')/\tau_l} \\
 & + \frac{\psi_0}{3\pi\eta} \int_{-\infty}^t dt' \mathbf{f}_0(t'). \quad (17)
 \end{aligned}$$

Here $3\pi\eta/\tau_l$ is the eigenvalue corresponding to the eigenfunction $\psi_l(s)$. The eigenfunction $\psi_0 = 1/\sqrt{2a}$ belongs to the eigenvalue $3\pi\eta/\tau_0 = 0$ and corresponds to the translational motion of the center of mass

$$\mathbf{r}_{cm}(t) \equiv \frac{1}{2a} \int_{-a}^a ds \mathbf{r}(s, t) = \frac{\psi_0}{3\pi\eta} \int_{-\infty}^t dt' \mathbf{f}_0(t'), \quad (18)$$

because $\int_{-a}^a ds \psi_l(s) = 0, \forall l \neq 0$. Assuming Gaussian distributed random forces $\mathbf{f}(s, t)$ characterized by the thermal average $\langle f_n(s, t) \rangle = 0$ and

$$\begin{aligned}
 \langle f_n(s, t) f_m(s', t') \rangle = & 6\pi\eta k_B T \delta_{nm} \delta(s - s') \delta(t - t'), \\
 & n, m \in \{x, y, z\} \quad (19)
 \end{aligned}$$

the translational diffusion coefficient $D_T(a)$ is of the form of eq 8:

$$\begin{aligned}
 D_T(a) \equiv & \lim_{t \rightarrow \infty} \frac{1}{6t} \langle (\mathbf{r}_{cm}(t) - \mathbf{r}_{cm}(0))^2 \rangle \\
 = & \frac{k_B T}{\eta} \frac{1}{6\pi a}. \quad (20)
 \end{aligned}$$

Hence $D_T(a)$ is independent of the local correlation length $1/p$ which is valid in the so-called free-draining

limit for dense polymer systems such as microgels.^{54,56,57} On the other hand, intramolecular hydrodynamic interactions lead to a dependence of $D_T(a)$ on $1/p$ in the case of dilute^{52,55,58} or semi-dilute^{61,62} polymer solutions.

The first internal mode ($l = 1$) exhibits the largest relaxation time and the rotational-fluctuation diffusion coefficient $\tilde{D}_R(a) = 1/(3\tau_1)$ can be derived as

$$\tilde{D}_R(a) = \frac{k_B T}{\eta} \frac{\alpha_1^4 + 4\alpha_1^2 p^2}{48\pi p} \quad (21)$$

$$\approx \begin{cases} \frac{k_B T}{\eta} \frac{1}{8\pi a^3} & , \quad pa \lesssim 0.02 \\ \frac{k_B T}{\eta} \frac{\pi p}{48a^2} & , \quad pa \gtrsim 2 \end{cases} \quad (22)$$

where α_1 follows from the transcendental equation

$$\alpha_1^3 \sin(\alpha_1 a) \cosh(\beta_1 a) - \beta_1^3 \cos(\alpha_1 a) \sinh(\beta_1 a) - 2p(\alpha_1^2 + \beta_1^2) \cos(\alpha_1 a) \cosh(\beta_1 a) = 0 \quad (23)$$

together with $\beta_1^2 - \alpha_1^2 = 4p^2$ and $\nu_0 = 3/(16k_B T)$, $\nu = 3/(8k_B T)$, $\epsilon_0 = 3/(16k_B T)$. The normalized rotational-fluctuation diffusion coefficient $\tilde{D}_R(a)/D_R(a, \alpha = 1)$ is plotted in Figure 7 as function of pa . In the stiff limit $pa \rightarrow 0$ the diffusion coefficient $\tilde{D}_R(a)$ agrees exactly with the rotational diffusion coefficient $D_R(a, \alpha = 1)$ of hard spheres. With decreasing stiffness (increasing values of pa) the ratio $\tilde{D}_R(a)/D_R(a, \alpha = 1)$ increases similar to the experimental findings presented in Table I. Hence shape fluctuations do indeed lead to a considerable increase of the diffusion coefficient $\tilde{D}_R(a)$.

Of course, the results shown in Figure 7 can only be considered to be of qualitative significance for the core-shell particles under consideration. However, these results clearly point to the importance of the coupling of rotational and internal modes in the case of soft materials. We emphasize that the core-shell particles maintain on average a spherical shape because $g_{VV}^{(2)}(q, t) - 1$ can be described by a single exponential function according to eq 6. Any permanent deviation from a spherical shape would lead to an additional term in eq 6 due to rotational motion.

Finally, it is worthwhile to compare the results of the present investigation with earlier studies of properties of microgels. A key feature of the static scattering intensity of both uniform microgel particles and core-shell microgel particles below the transition temperature is a strong scattering signal that is due to collective fluctuations of the polymer gel.^{10,13,21} It has been demonstrated that the contribution of this internal dynamics to the static scattering intensity vanishes for temperatures above the transition temperature $T=32^\circ\text{C}$ (see Figure 4 in ref²¹). The corresponding collective dynamic fluctuations of the PNIPA network below the LCST have been measured using DLS^{60,63} and neutron spin-echo spectroscopy.⁶⁴ Despite the different q range of the two methods, the found

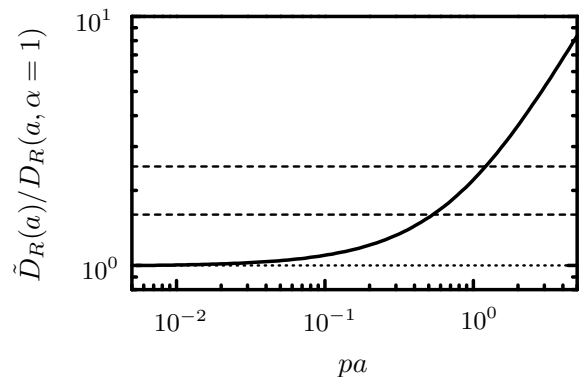


FIG. 7: The reduced rotational-fluctuation diffusion coefficient $\tilde{D}_R(a)/D_R(a, \alpha = 1)$ according to eqs 21 and 9 as a function of pa characterizing the stiffness of the model described in the main text. In the stiff limit $pa \rightarrow 0$ the rotational-fluctuation diffusion coefficient $\tilde{D}_R(a)$ reduces to the rotational diffusion coefficient $D_R(a, \alpha = 1)$ of hard spheres. The deviations of $\tilde{D}_R(a)/D_R(a, \alpha = 1)$ from the value 1 increase with decreasing stiffness, i.e., increasing values of pa , due to additional internal dynamics. The dashed lines mark the values $\alpha = 1.6$ and $\alpha = 2.5$ as obtained from the experimental data at $T = 25^\circ\text{C}$ and $T = 15^\circ\text{C}$ (see Table I).

collective diffusion coefficient of the network has a similar order of magnitude. This most likely indicates that the network motion is always observable independent of the characteristic length scale of the experiment. Hence, the deviations from the hard sphere model observed in the present study by means of DDLS can be considered as a manifestation of these fluctuations. Very recently it has been demonstrated experimentally that the softness of microgel particles has also a pronounced influence on the dynamics in concentrated microgel suspensions.⁶⁵

V. CONCLUSION

In conclusion, our findings elucidate an important and interesting interplay between shape fluctuations and rotational motion of deformable objects which profoundly affects their dynamics. The control over the degree of deformations offered by varying the temperature should make the core-shell microgels useful for fundamental studies in statistical physics. We anticipate that the results obtained for the present system is of general importance for a better understanding for more complicated systems related to biophysics as e.g. vesicles.

VI. ACKNOWLEDGMENT

Financial support by the Deutsche Forschungsgemeinschaft, SFB 481, Bayreuth, and by the Schwerpunktprogramm Hydrogele is gratefully acknowledged.

- ¹ Hu, Z.; Chen, Y.; Wang, C.; Zheng, Y.; Li, Y. *Nature* **1998**, 393, 149-152.
- ² Juodkazis, S.; Mukai, N.; Wakaki, R.; Yamaguchi, A.; Matsuo, S.; Misawa, H. *Nature* **2000**, 408, 178-181.
- ³ Nayak, S.; Lyon, L. A. *Angew. Chem. Int. Ed.* **2005**, 44, 7686-7708.
- ⁴ Dong, L.; Agarwal, A. K.; Beebe, D. J.; Jiang, H. *Nature* **2006**, 442, 551-554.
- ⁵ Chu, L.-Y.; Kim, J.-W.; Shah, R. K.; Weitz, D. A. *Adv. Funct. Mater.* **2007**, 17, 3499-3504.
- ⁶ Ballauff, M.; Lu, Y. *Polymer* **2007**, 48, 1815-1823.
- ⁷ Contreras-Cáceres, R.; Sánchez-Iglesia, A.; Karg, M.; Pastoriza-Santos, I.; Pérez-Juste, J.; Pacifico, J.; Hellweg, Th.; Fernández-Barbero, A.; Liz-Marzán, L. M. *Advanced Mater.* **2008**, 20, 1666-1670.
- ⁸ Karg, M.; Pastoriza-Santos, I.; Pérez-Juste, J.; Hellweg, Th.; Liz-Marzán, L. M. *Small*, **2007**, 3, 1222-1229.
- ⁹ Schmidt, S.; Motschmann, H.; Hellweg, Th.; von Klitzing, R. *Polymer* **2008**, 49, 749-756.
- ¹⁰ Dingenouts, N.; Norhausen, Ch.; Ballauff, M. *Macromolecules* **1998**, 31, 8912-8917.
- ¹¹ Duracher, D.; Sauzedde, F.; Elaissari, A.; Perrin, A.; Pichot, C. *Coll. Polym. Sci.*, **1998**, 276, 219-231.
- ¹² Duracher, D.; Sauzedde, F.; Elaissari, A.; Pichot, C.; Nabzar, K. *Coll. Polym. Sci.*, **1998**, 276, 920-929.
- ¹³ Seelenmeyer, S.; Deike, I.; Rosenfeldt, S.; Norhausen, Ch.; Dingenouts, N.; Ballauff, M.; Narayanan, T.; Lindner, P. *J. Chem. Phys.* **2001**, 114, 10471-10478.
- ¹⁴ Hellweg, Th.; Dewhurst, C. D.; Eimer, W.; Kratz, K. *Langmuir*, **2004**, 20, 4330-4335.
- ¹⁵ Crassous, J.; Siebenbürger, M.; Ballauff, M.; Drechsler, M.; Henrich, O.; Fuchs, M. *J. Chem. Phys.* **2006**, 125, 204906-1-11.
- ¹⁶ Crassous, J.; Siebenbürger, M.; Ballauff, M.; Drechsler, M.; Hajnal, D.; Henrich, O.; Fuchs, M. *J. Chem. Phys.* **2008**, 128, 204902-1-16.
- ¹⁷ Shibayama, M.; Tanaka, T.; Han, C. C. *J. Chem. Phys.* **1992**, 97, 6829-6841.
- ¹⁸ Pelton, R. *Adv. Colloid Interf. Sci.* **2000**, 85, 1-33.
- ¹⁹ Tanaka, T.; Sato, E.; Hirokawa, Y.; Hirotsu, S.; Peetermans, J. *Phys. Rev. Lett.* **1985**, 55, 2455-2458.
- ²⁰ Wu, J. Z.; Zhou B.; Hu, Z. B. *Phys. Rev. Lett.* **2003**, 90, 048304-1-4.
- ²¹ Kratz, K.; Hellweg, Th.; Eimer, W. *Polymer* **2001**, 42, 6631-6639.
- ²² Huang, J. S.; Milner, S. T.; Farago, B.; Richter, D. *Phys. Rev. Lett.* **1987**, 59, 2600-2603.
- ²³ Farago, B.; Richter, D.; Huang, J. S.; Safran, S. A.; Milner, S. T. *Phys. Rev. Lett.* **1990**, 65, 3348-3351.
- ²⁴ Gang, H.; Krall, A. H.; Weitz, D. A. *Phys. Rev. Lett.* **1994**, 73, 3435-3438.
- ²⁵ Hellweg, Th.; Langevin, D. *Phys. Rev. E* **1998**, 57, 6825-6834.
- ²⁶ Kantsler, V.; Segre, E.; Steinberg, V. *Phys. Rev. Lett.* **2007**, 99, 178102-1-4.
- ²⁷ Turitsyn, K. S.; Vergeles, S. S. *Phys. Rev. Lett.* **2008**, 100, 028103-1-4.
- ²⁸ Abkarian, M.; Lartigue, C.; Viallat, A. *Phys. Rev. Lett.* **2002**, 88, 068103-1-4.
- ²⁹ Kantsler V.; Steinberg V. *Phys. Rev. Lett.* **2005**, 95, 258101-1-4.
- ³⁰ Noguchi H.; Gompper, G. *Phys. Rev. Lett.* **2007**, 98, 128103-1-4.
- ³¹ Lebedev, V. V.; Turitsyn, K. S.; Vergeles, S. S. *Phys. Rev. Lett.* **2007**, 99, 218101-1-4.
- ³² Berne, B.; Pecora, R. *Dynamic Light Scattering*, Wiley: New York, 1976.
- ³³ Schmitz, K. S. *An Introduction to Dynamic Light Scattering by Macromolecules*, Academic Press: London, 1990.
- ³⁴ Crowther, H. M.; Saunders, B. R.; Mears, S. J.; Cosgrove, T.; Vincent, B.; King, S. M.; Yu, G. E. *Colloids Surf. A.*, **1999**, 152, 327-333.
- ³⁵ Wu, J. Z.; Huang, G.; Hu, Z. *Macromolecules* **2003**, 36, 440-448.
- ³⁶ Berndt, I.; Richtering, W. *Macromolecules* **2003**, 36, 8780-8785.
- ³⁷ Stieger, M.; Richtering, W.; Pedersen, J. S.; Linder, P. *J. Chem. Phys.* **2004**, 120, 6197-6206.
- ³⁸ Mason, T. G.; Lin, M. Y. *Phys. Rev. E* **2005**, 71, 040801-1-4.
- ³⁹ Berndt, I.; Pedersen, J. S.; Linder, P.; Richtering, W. *Langmuir* **2006**, 22, 459-468.
- ⁴⁰ Berndt, I.; Pedersen, J. S.; Richtering, W. *Ang. Chem. Int. Ed.* **2006**, 45, 1737-1741.
- ⁴¹ Zhao, X.; Hong, W.; Suo, Z; *Appl. Phys. Lett.* **2008**, 92, 051904-051907.
- ⁴² Lu, Y.; Mei, Y.; Drechsler, M.; Ballauff, M. *Ang. Chem. Int. Ed* **2006**, 45, 813-816.
- ⁴³ Mei, Y.; Lu, Y.; Polzer, F.; Ballauff, M.; Drechsler, M. *Chem. Mater.* **2007**, 19, 1062-1069.
- ⁴⁴ Crassous, J.; Ballauff, M.; Drechsler, M.; Schmidt, J.; Talmon, Y. *Langmuir* **2006**, 22, 2403-2406.
- ⁴⁵ Crassous, J.; Wittemann, A.; Siebenbürger, M.; Schrunner, M.; Drechsler, M.; Ballauff, M. *Colloid Polym. Sci.* **2008**, 286, 805-812.
- ⁴⁶ Pecora R. *J. Chem. Phys.* **1968**, 49, 1036-1043.
- ⁴⁷ Koenderink, G. H.; Philipse, A. P. *Langmuir* **2000**, 16, 5631-5638.
- ⁴⁸ Eimer, W.; Dorfmueller, T. *J. Phys. Chem.* **1992**, 96, 6790-6800.
- ⁴⁹ Degiorgio, V.; Piazza, R.; Corti, M.; Stavans, J. *J. Chem. Soc. Faraday Trans.* **1991**, 87, 431-434.
- ⁵⁰ Pecora R.; Steele W. A. *J. Chem. Phys.* **1965**, 42, 1872-1879.
- ⁵¹ Carrasco, B; Garcia de la Torre, J. *Biophys. J.* **1999**, 75, 3044-3057.
- ⁵² Harnau, L.; Winkler, R. G.; Reineker, P. *Macromolecules* **1999**, 32, 5956-5960.
- ⁵³ Hu, C.-M.; Zwanzig, R. *J. Chem. Phys.* **1974**, 60, 4354-4357.
- ⁵⁴ Harnau, L.; Winkler, R. G.; Reineker, P. *J. Chem. Phys.* **1995**, 102, 7750-7757.
- ⁵⁵ Harnau, L.; Winkler, R. G.; Reineker, P. *J. Chem. Phys.* **1996**, 104, 6355-6368.
- ⁵⁶ Harnau, L.; Winkler, R. G.; Reineker, P. *Europhys. Lett.* **1999**, 45, 488-494.
- ⁵⁷ Harnau, L.; Winkler, R. G.; Reineker, P. *Phys. Rev. Lett.* **1999**, 82, 2408-2408.
- ⁵⁸ Harnau, L.; Reineker, P. *New J. Phys.* **1999**, 1, 3.1-3.6.
- ⁵⁹ Winkler, R. G. *Phys. Rev. Lett.* **2006**, 97, 128301-1-4.
- ⁶⁰ Wu, C.; Zhou, S. *Macromolecules* **1996**, 29, 1574-1578
- ⁶¹ Harnau, L. *J. Chem. Phys.* **2001**, 115, 1943-1945.

- ⁶² Bolisetty, S.; Airaud, C.; Xu, Y.; Müller, A. H. E.; Harnau, L.; Rosenfeldt, S.; Lindner, P.; Ballauff, M. *Phys. Rev. E* **2007**, 75, 040803(R)-1-4.
- ⁶³ Yang, C.; Kizhakkedathu, J. N.; Brooks, D. E.; Jin, F.; Wu, C. *J. Phys. Chem. B* **2004**, 108, 18479-18484.
- ⁶⁴ Hellweg, Th.; Kratz, K.; Pouget, S.; Eimer, W. *Colloids Surf. A* **2002**, 202, 223-232.
- ⁶⁵ Eckert, T.; Richtering, W. *J. Chem. Phys.* **2008**, 129, 124902-1-6.